

RAPID INFRARED VARIABILITY OF THREE RADIO-LOUD NARROW-LINE SEYFERT 1 GALAXIES: A VIEW FROM THE *WIDE-FIELD INFRARED SURVEY EXPLORER*

NING JIANG^{1,2}, HONG-YAN ZHOU^{1,2,3}, LUIS C. HO⁴, WEIMIN YUAN⁵, TING-GUI WANG^{1,2},
XIAO-BO DONG^{1,2}, PENG JIANG^{1,2}, TUO JI³ AND QIGUO TIAN³

To appear in The Astrophysical Journal Letters.

ABSTRACT

Using newly released data from the *Wide-field Infrared Survey Explorer*, we report the discovery of rapid infrared variability in three radio-loud narrow-line Seyfert 1 galaxies (NLS1s) selected from the 23 sources in the sample of Yuan et al. (2008). J0849+5108 and J0948+0022 clearly show intraday variability, while J1505+0326 has a longer measurable time scale within 180 days. Their variability amplitudes, corrected for measurement errors, are $\sim 0.1 - 0.2$ mag. The detection of intraday variability restricts the size of the infrared-emitting region to $\sim 10^{-3}$ pc, significantly smaller than the scale of the torus but consistent with the base of a jet. The three variable sources are exceptionally radio-loud, have the highest radio brightness temperature among the whole sample, and all show detected γ -ray emission in *Fermi*/LAT observations. Their spectral energy distributions resemble those of low-energy-peaked blazars, with a synchrotron peak around infrared wavelengths. This result strongly confirms the view that at least some radio-loud NLS1s are blazars with a relativistic jet close to our line of sight. The beamed synchrotron emission from the jet contributes significantly to and probably dominates the spectra in the infrared and even optical bands.

Subject headings: galaxies: individual (SDSS J084957.98+510829.0, SDSS J094857.32+002225.5, SDSS J150506.48+032630.8) — galaxies: active — galaxies: jets — infrared: galaxies

1. INTRODUCTION

Active galactic nuclei (AGNs; including Seyfert galaxies and quasars), powered by accretion onto supermassive black holes, show multiwavelength variability on time scales from years to less than a day. As one of the first recognized properties of quasars, variability has served as an important tool to investigate the emission processes of AGNs (e.g., Ulrich et al. 1997; Peterson 2001). In particular, intraday variability can provide essential constraints on the central regions of AGNs on physical scales smaller than the Solar System, which in general cannot be resolved directly by current observational capabilities. Intraday variability has been detected throughout nearly the entire observable electromagnetic spectrum in many radio-loud AGNs with flat radio spectra, which are often collectively called blazars (see review in Wagner & Witzel 1995). Radio-loud AGNs plausibly contain a relativistic jet originating near the central black hole. Blazars are believed to be those with a relativistic jet oriented close to the line of sight; thus, their nonthermal jet emission is highly Doppler boosted.

Narrow-line Seyfert 1 galaxies (NLS1s), originally defined by Osterbrock & Pogge (1985), are a special class of AGNs in which the broad permitted lines are relatively narrow and the [O III] $\lambda 5007$ emission line is weak (see Pogge 2000 for a review). Apart from this, NLS1s also show strong Fe II emission lines in their optical/ultraviolet spectra, steep soft X-ray spectra, and rapid X-ray variability (Boller et al. 1996; Leighly 1999; Sulentic et al. 2000; Zhou et al. 2006). Zhou & Wang (2002) found that the fraction of radio-loud objects among NLS1s ($\sim 6\%$) is significantly less than that found in normal type 1

quasars ($\sim 13\%$). Very radio-loud NLS1s, those with radio-loudness parameter $R > 100$, where R is commonly defined as the ratio of the radio flux density at 6 cm to optical flux density at 4400 Å (Kellermann et al. 1989), are extremely rare, comprising only 2.5% of the NLS1 population (Komossa et al. 2006). Of particular interest, some individual objects are found to exhibit blazar-like behavior (e.g., Zhou et al. 2003, 2005, 2006; Gallo et al. 2006). Yuan et al. (2008) presented a comprehensive study of 23 genuine radio-loud NLS1s (hereinafter the Y08 sample). The radio sources in radio-loud NLS1s are ubiquitously compact, unresolved on scales of several arcseconds. Some of them show interesting properties, including flat radio spectra, compact VLBI cores, very high radio brightness temperatures (T_B), enhanced optical continuum emission, flat X-ray spectra, large-amplitude X-ray flux and spectral variability, and blazar-like spectral energy distributions (SEDs). Based on recent observations taken by *Fermi* Gamma-ray Space Telescope (*Fermi*), some of the radio-loud NLS1s indeed display a hard X-ray component and prominent γ -ray radiation, which undoubtedly arise from a relativistic jets pointed toward us (Abdo et al. 2009a, 2009b; Foschini et al. 2011). The blazar interpretation of radio-loud NLS1s appears to be successful, but additional evidence is still needed for the majority of the class. Flat and inverted radio spectra are also often seen in some normal Seyfert galaxies, although most have much less power compared to the objects studied in the Y08 sample (e.g., Ho & Ulvestad 2001).

As a general feature of blazars, intraday variability is expected in radio-loud NLS1s if the above interpretation is true. This has been confirmed by some optical intra-night

¹Key laboratory for Research in Galaxies and Cosmology, University of Science and Technology of China, Chinese Academy of Science, Hefei, Anhui 230026, China; jnac@mail.ustc.edu.cn

²Department of Astronomy, University of Science and Technology of China, Hefei, Anhui 230026, China

³Polar Research Institute of China, 451 Jinqiao Road, Pudong, Shanghai 200136, China

⁴The Observatories of the Carnegie Institution for Science, 813 Santa Barbara Street, Pasadena, CA 91101, USA

⁵National Astronomical Observatories, Chinese Academy of Sciences, Beijing 100012, China

Table 1. *WISE* Data

Name (1)	z (2)	W1 (3)	W2 (4)	W3 (5)	W4 (6)	Δ_{W1} (7)	Δ_{W2} (8)	Δ_{W3} (9)	var_flag (10)	$\log R_{1.4}$ (11)	$\log T_B$ (12)
J0849+5108	0.583	14.03±0.03	13.14±0.03	10.04±0.05	7.54±0.11	0.11±0.02	0.19±0.03	0.15	4610	3.16	13.0
J0948+0022	0.584	13.22±0.03	12.12±0.02	9.15±0.04	6.78±0.08	0.19±0.01	0.18±0.02	0.16	9903	2.55	12.7
J1505+0326	0.408	14.04±0.03	13.10±0.03	9.89±0.04	7.12±0.07	0.08±0.02	0.13±0.03	0.12	6730	3.19	14.0
others (median)	0.523	14.36±0.03	13.43±0.03	10.52±0.06	8.17±0.11	0.02±0.03	0.05±0.05	0.00	0100	2.53	...

Note. — Col.(1): abbreviated name of object used in this paper and median value of the other 20 sources. Col.(2): redshift. Col.(3)–(6): W1–W4 magnitude from *WISE* All-Sky Source Catalog. Col.(7)–(9): Δ of W1–W3 magnitudes, where the error is given by the median Δ of standard stars with similar magnitudes. Col.(10): variability flag. Col.(11): logarithm of radio-loudness parameter defined as $R_{1.4} \equiv f_\nu(1.4 \text{ GHz})/f_\nu(4400 \text{ \AA})$, where $R_{1.4} = 1.9R$ for a radio index $\alpha = -0.5$. Col.(12): logarithm of radio brightness temperature (K). Some other related information can be found in Y08.

observations (e.g., Liu et al. 2009; Shi & Shan 2011). Extending such an investigation to the infrared (IR) becomes widely possible only after the recent mission of *Wide-field Infrared Survey Explorer* (*WISE*; Wright et al. 2010), which achieves a sensitivity in the $12 \mu\text{m}$ band more than 100 times higher than the most comparable previous mission *Infrared Astronomical Satellite* (*IRAS*). Indeed, all 23 objects in the Y08 sample are detected by *WISE* but none of them except one (SDSS J163323.58+471859.0, hereinafter J1633+4718)⁶ was detected by *IRAS*. *WISE* has mapped the entire sky in four bands centered at 3.4, 4.6, 12, and $22 \mu\text{m}$ (hereinafter the W1, W2, W3, and W4 bands) with angular resolutions of $6''.1$, $6''.4$, $6''.5$, and $12''$, respectively. The field-of-view of *WISE* is $47' \times 47'$ and has a small (10%) overlap between adjacent fields in one orbit. The scan circle advances by about $4'$ per orbit. Thus, there are typically 12 successive orbits covering a given source. With ~ 15 orbits per day, the observing cadence of *WISE* is well suited for studying intraday variability. It is worth noting that the perspective from IR variability has some unique advantages. First, light in the IR is much less affected by dust extinction and/or gas absorption than in the optical, UV, or X-ray bands. Even compared with radio, IR is free from contamination from refractive interstellar scintillation, which is wavelength-dependent in the radio but negligible in the IR.

This Letter reports the discovery of rapid IR variability in three radio-loud NLS1s selected from the Y08 sample using recently released data from *WISE*. We assume a cosmology with $H_0 = 70 \text{ km s}^{-1} \text{ Mpc}^{-1}$, $\Omega_m = 0.3$, and $\Omega_\Lambda = 0.7$.

2. DATA ANALYSIS AND RESULTS

The *WISE* All-Sky Data Release Source Catalog contains position and four-band photometric data for 563,921,584 objects detected on the coadded atlas images (Cutri et al. 2012). Photometry was performed by fitting point-spread functions (PSFs) simultaneously to all the individual exposures covering an object. A variability flag, var_flag , is assigned to every source in each band, giving the probability of flux variation as represented by an integer value from 0 to 9. A value of 0 indicates insufficient or inadequate data to determine the variability probability, while values from 1 to 9 indicate increas-

ing likelihood of variability (see Hoffman et al. 2012 for details). According to var_flag in the *WISE* catalog, there are three radio-loud NLS1s in the Y08 sample with probable variability: SDSS J084957.98+510829.0 (hereinafter J0849+5108), SDSS J094857.32+002225.5 (hereinafter J0948+0022), and SDSS J150506.48+032630.8 (hereinafter J1505+0326), whose respective variability flags are “4610,” “9903,” and “6730.” For the remaining 20 sources, the variability flags are no larger than 2 in any of the four bands. The data for these sources are presented in Table 1.

We first examine the photometric errors of the *WISE* data using standard stars⁷ chosen from the SDSS Stripe 82 catalog (Ivezić et al. 2007). The single-frame photometric data can be downloaded from *WISE* All-Sky Single Exposure (L1b) Source Table via the GATOR query service of the NASA/IPAC Infrared Science Archive⁸. We adopt the PSF profile-fit photometric magnitudes⁹. The magnitude standard deviation Σ for a given star in a band is calculated as

$$\Sigma = \sqrt{\frac{1}{n-1} \sum_{i=1}^N (m_i - \langle m \rangle)^2}, \quad (1)$$

where $\langle m \rangle$ is the flux-weighted mean. Figure 1 displays Σ as function of magnitude in W1 and W2 for about 5000 stars. We have also overplotted the 23 radio-loud NLS1s. The three candidate variable sources from the Y08 sample, as well as another one (SDSS J172206.03+565451.6, hereinafter J1722+5654), have large variance outside the $1\text{-}\sigma$ scatter of the Σ -magnitude distribution; these outliers are either intrinsically variable or their observations have large systematic errors.

We begin by extracting the light curves to reexamine the variability of the three candidate variable objects. The signal-to-noise ratio (S/N) is high enough to give reliable photometric measurement with $S/N > 10$ in W1 and W2 and $S/N > 5$ in W3 for all exposures. Judging by the reduced chi-square (χ^2) of the profile-fit photometry, which is close to 1, the PSF fitting is reliable and there is little contamination from nearby objects. Unfortunately, the W4 data have much lower S/N and larger photometric errors; some are marked as “null,” which means that it is either not measurable or only an upper limit

⁶However, the *IRAS* source is most likely associated with the star-forming nuclei of a companion galaxy, separated by $\sim 4''$ from the AGN (Yuan et al. 2010).

⁷<http://www.astro.washington.edu/users/ivezic/sdss/catalogs/stripe82.html>

⁸<http://irsa.ipac.caltech.edu/cgi-bin/Gator/nph-dd>

⁹Brief description of the definition of profile-fit magnitude as well as other related parameters can be found in Cutri et al. (2012).

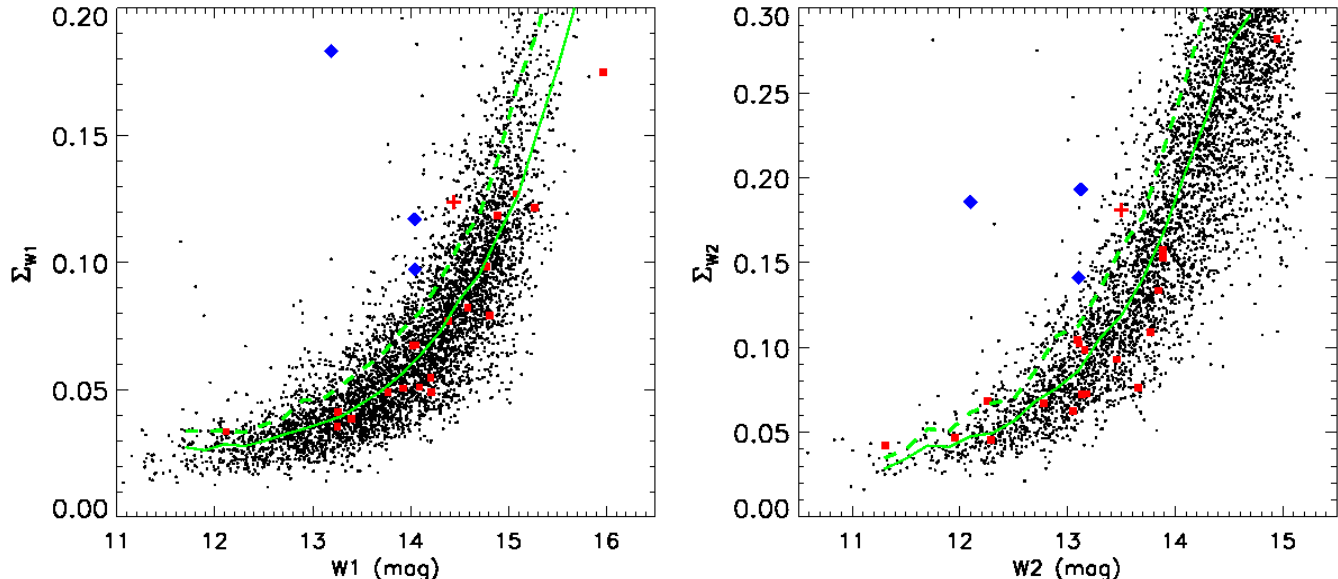


FIG. 1.— Standard deviation of single-frame photometric measurements as a function of magnitude for the W1 (left) and W2 (right) band. Black dots are standard stars from SDSS Stripe 82; its median values and 1- σ upper boundary are marked with the green solid and dashed lines, respectively. The three candidate variable sources in the Y08 sample are plotted with blue diamonds, J1722+5654 as a red plus, and the nonvariable sources in our sample as red squares.

can be placed on the flux. We exclude the W4 data from further analysis. In light of possible photometric zero point offsets in different fields, for every source we choose as “standards” in the field 30–50 stars with brightness comparable to that of the source. For each standard star, we calculate the differential magnitude between a single observation and the flux-weighted mean magnitude. Then we take the zero point offset for a given field as the mean differential magnitude of all the standard stars in the field. The offsets in W1 and W2 are tiny, typically <0.02 mag with a systematic error of ~ 0.01 mag. Most of the standard stars are too faint in W3, and thus we could not determine a zero point offset for this band

The variability amplitude is commonly measured by the variance of the observed magnitudes, with the contribution from measurement errors subtracted. We adopt a formalism similar to that used in Ai et al. (2010; see also Sesar et al. 2007), whereby

$$\Delta = \begin{cases} (\Sigma^2 - \xi^2)^{1/2}, & \text{if } \Sigma > \xi, \\ 0, & \text{otherwise.} \end{cases} \quad (2)$$

Here the measurement error ξ includes both the 1- σ profile-fit photometric error and the systematic error from zero point offsets (ξ_{zero} for W1 and W2, which is, in any case, almost negligible):

$$\xi^2 = \frac{1}{N} \sum_{i=1}^N \xi_i^2 + \xi_{\text{zero}}^2. \quad (3)$$

Figure 2 shows the final light curves for the three sources for which variability has been detected. In summary:

- *J0849+5108* — There are 15 exposures within 1.2 days, yielding $\Delta_{W1} = 0.11$, $\Delta_{W2} = 0.19$, and $\Delta_{W3} = 0.15$. As a comparison, the standard stars with similar magnitudes in W1 and W2 give a median value of $\Delta_{W1} = 0.02$ and $\Delta_{W2} = 0.03$.
- *J0948+0022* — The 10 exposures within one day give $\Delta_{W1} = 0.19$, $\Delta_{W2} = 0.18$, and $\Delta_{W3} = 0.16$. The standard

stars with similar magnitudes yield a median value of $\Delta_{W1} = 0.01$ and $\Delta_{W2} = 0.02$.

- *J1505+0326* — This target was observed during two epochs separated by about 180 days. No evident intraday variability can be seen in either single epoch ($\Delta_{W1,W2,W3} \approx 0$), but the magnitude jump between the two epochs is considerable (see the bottom panel of Figure 2). The flux-weighted mean W1 and W2 magnitudes varied by 0.16 and 0.25 between the two epochs, while the observations for both epochs as a whole yield $\Delta_{W1} = 0.08$, $\Delta_{W2} = 0.13$, and $\Delta_{W3} = 0.12$. The W1 and W2 magnitudes are almost equal to those of J0849+5108, and the Δ of standard stars is also comparable to that for J0849+5108. Given the redshift of 0.408, the time scale of variability should be shorter than 128 days in the source rest frame.

To verify the accuracy of the variability flag assigned by *WISE*, we recomputed the variability probability following the formalism devised by Hoffman et al. (2012), but using our own error estimates. With the exception of J1633+4718, which shows likely variability according to our test, our results are consistent with those of Hoffman et al (2012). The PSF profile-fit magnitudes for J1633+4718, however, are probably unreliable because this source is an interacting system of two galaxies separated by $\sim 4''$ as denoted above, which still cannot be resolved by *WISE*. By contrast, J1722+5654, which shows a large magnitude deviation (red plus symbol in Figure 1), has $\Delta \approx 0$ after correction for systematic measurement errors.

Lastly, we performed a cross correlation analysis for the three variable sources to search for evidence of time lag between the light curves of the three bands. No significant lag was found.

3. DISCUSSION AND CONCLUSIONS

Using newly released data from *WISE*, whose well-designed observation mode provides a modest number of repeat obser-

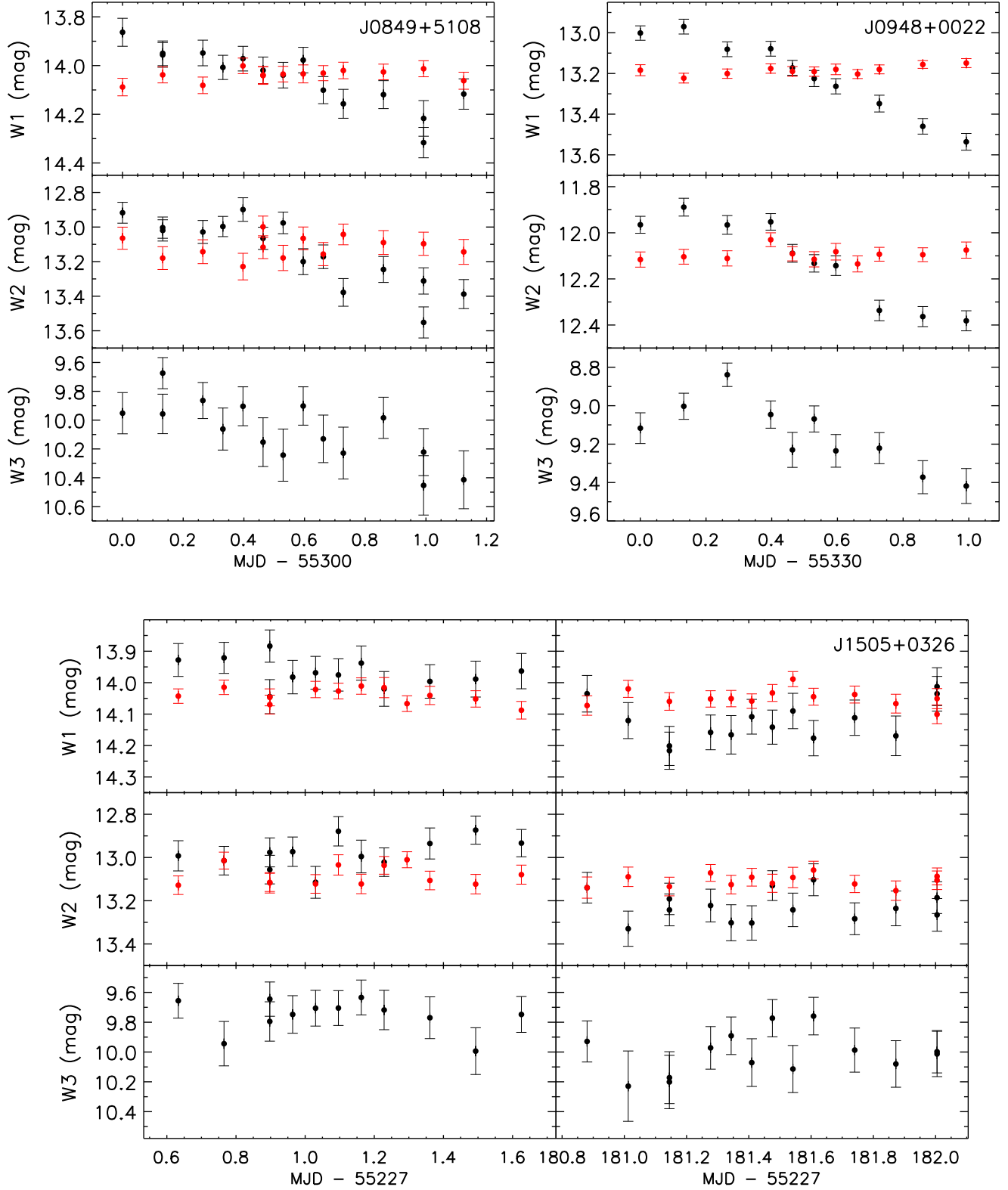


FIG. 2.— WISE light curves constructed from profile-fit magnitudes; $1\text{-}\sigma$ error bar are plotted. The red points in the W1 and W2 bands represent measurements from a typical nearby “standard” star, shifted slightly by a constant for ease of comparison.

variations of the sky, we discovered significant IR variability in three out of 23 radio-loud NLS1s selected from the sample of Y08. All three are markedly variable in the W1 ($3.4\ \mu\text{m}$) and/or

W2 ($4.6\ \mu\text{m}$) bands, at greater than 6σ confidence. Closer examination of their light curves reveals that J0849+5108 and J0948+0022 show clear intraday variability, while J1505+0326

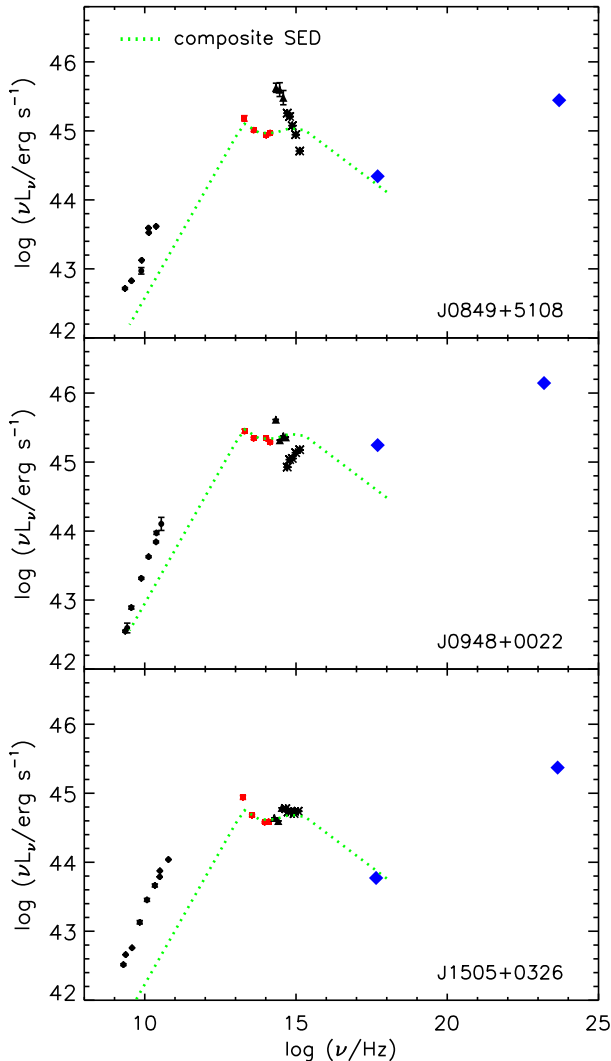


FIG. 3.— SEDs of the three variable objects. Data include radio measurements (black dots), *WISE* photometry (red squares), 2MASS near-IR magnitudes (black triangles), SDSS *ugriz* PSF magnitudes corrected for Galactic extinction (black stars), X-ray and γ -ray from Abdo et al. 2009b; D’Ammando et al. 2012 (blue diamonds). The mean SED of the other 20 nonvariable sources is plotted with a green dotted line. The radio, 2MASS, and SDSS data were collected from NED.

varies on a longer time scale of 180 days or less. Quantifying the variability amplitude using the variance of the observed magnitudes (e.g., Ai et al. 2010), after accounting for measurement errors, we find $\Delta \approx 0.1 - 0.2$. This represents the first definitive detection of IR intraday variability for radio-loud NLS1s.

The variability time scale allows us to place limits on the size of the IR-emitting region. In the case of J1505+0326, for which only relatively long-term variability can be determined, the size of emission region is confined to be $\lesssim 0.1$ pc. On the other hand, the detection of intraday variability in J0849+5108 and J0948+0022 implies that their IR emission region is very compact, confined to scales of $\sim 10^{-3}$ pc, which corresponds to only hundreds of Schwarzschild radii assuming $M_{\text{BH}} \approx 3 \times 10^7 M_{\odot}$ (Y08). Thermal IR radiation in AGNs is normally believed to be arise mainly from a dusty torus outside of the dust sublimation radius (Laor & Draine 1993), which for graphite grains is about 0.5 pc for these three sources. If the inferred size of the emission region for J0849+5108 and J0948+0022 is representative, it implies that the IR radiation comes from a spa-

tial scale much smaller than that of the torus, perhaps no larger than that of the accretion disk. This strongly suggests that the IR emission is dominated by an additional nonthermal component, presumably associated with the jet responsible for the radio emission. Coincidentally, but perhaps not surprisingly, in all three objects variable γ -ray emission has been detected recently with *Fermi*/LAT (Abdo et al. 2009a, 2009b; Foschini 2011; D’Ammando et al. 2012). This confirms the blazar-like nature of these three radio-loud NLS1s and supports the hypothesis that they do indeed have relativistic jets pointing close to our line of sight. In this scenario, the variable IR emission derives from synchrotron radiation from the base of the jet.

We note, in passing, that intraday variability of J0948+0022 with similar amplitude as seen in *WISE* has been reported also in the optical (Liu et al. 2010). IR observations are, in principle, superior to optical observations for the purposes of detecting synchrotron radiation from jets. IR radiation is less affected by dust extinction and is less contaminated by AGN accretion processes that may cause optical variability due to instabilities in the accretion flow.

The fraction of IR-variable sources in the Y08 sample seems to be quite low (3/23 or 13%). One immediate, trivial reason is probably simply sensitivity. About half of the Y08 sample is fainter than the three variable sources, and their variability, if present, is likely masked by measurement errors (cf. Figure 1). The degree of radio-loudness also seems to matter. The majority of the parent sample have radio-loudness parameters much lower than those of J0849+5108 and J1505+0326. J0948+0022 has a R parameter 0.6 dex lower than the other two variable objects, but it is still higher than half of the full sample (see Table 1 and Figure 3). According to Y08, eight sources display prominent radio variability between two epochs separated by several years. The three IR variables discussed here show the largest amplitude of radio variations ($\sim 40\% - 75\%$) and the highest radio brightness temperatures, all exceeding the threshold value, usually estimated to be $T_{\text{B}} \simeq 10^{12}$ K, above which inverse-Compton catastrophe is predicted to occur (Kellermann & Pauliny-Toth 1969). Taking the inverse-Compton limit of 10^{12} K as a conservative limit, the minimum Doppler factors are estimated to be 1.5–4.7, which are within the range of values for relativistic jets inferred for classical radio-loud AGNs (Ghisellini et al. 1993). In addition, they show ubiquitously inverted radio spectra and happen to be the flattest three of the 11 sources whose radio spectral slope have been estimated in Y08, which is consistent with the blazar nature.

Selection by IR variability also must favor objects that are intrinsically more IR luminous. The overall SED of blazars is characterized by two broad bumps due to synchrotron emission and inverse-Compton scattering, respectively. “Blazars” is a collective term for BL Lac objects and flat-spectrum radio quasars (FSRQs), which are distinguished from each other according to the strength of their emission lines in optical spectra: BL Lac objects have very weak emission lines while FSRQs look like normal quasars. Depending on the peak frequency of the synchrotron bump, BL Lac objects can be divided into low-energy-peaked sources, whose SEDs reach a local maximum at IR–optical wavelengths, and high-energy-peaked ones, which peak near the UV or soft X-ray band (Giommi & Padovani 1994). Similarly, FSRQs can also be divided into their high-frequency-peaked and low-frequency-peaked varieties, parallel to the classification devised for BL Lac objects (Perlman et al. 1998). Our three IR-variable radio-loud NLS1s have SEDs that,

in fact, peak near the IR (Figure 3) and qualitatively resemble low-frequency-peaked FSRQs in terms of their overall energy distribution. (We note that the apparent discontinuity between the IR and optical data points on the SED may be caused by variability, since the IR and optical data were not taken contemporaneously.) This strongly suggests that our IR selection preferentially favors systems with IR-peaked SEDs.

Two tests support the above hypothesis. First, we examined the IR variability properties of the large sample of BL Lac objects from Nieppola et al. (2006). Judging from the *var_flg* parameter from *WISE*, 24 out of the 98 low-energy-peaked sources can be considered variable (*var_flg* > 5) in at least one *WISE* band, whereas, strikingly, only 6 of 110 high-energy-peaked source qualify as variable. As in our sample, it appears that the higher incidence of IR variability is related to the higher IR/optical flux contribution from jets. Further evidence comes from examining the strengths of the optical emission lines. The median equivalent width of H β for the three IR-variable radio-loud NLS1s (23 Å) is significantly smaller than not only the median value of all quasars (~ 70 Å; Zhou et al. 2006; Shen et al. 2011) but also that of the parent sample of radio-loud NLS1s (42 Å). This is consistent with the notion that IR-variable sources have a stronger optical continuum due

to enhanced contribution from a jet.

This study demonstrates that the *WISE* All-Sky Survey affords an excellent opportunity to study IR variability in AGNs, a powerful diagnostic of their radiation mechanism. Short-term IR variability, in particular, is sensitive to spatial scales relevant to the base of the jet, providing an effective and efficient probe that complements radio and high-energy observations. We will take full use of the *WISE* data to study other classes of AGNs in the near future.

This work is supported by Chinese Natural Science Foundation through projects NSF-10973012, NSF-11033007, SOC project CHINARE2012-02-03 and Fundamental Research Funds for the Central Universities with grant WK 2030220006. The research of LCH is supported by the Carnegie Institution for Science. This publication makes use of data products from the Wide-field Infrared Survey Explorer, which is a joint project of the University of California, Los Angeles, and the Jet Propulsion Laboratory/California Institute of Technology, funded by the National Aeronautics and Space Administration. This research has made use of the NASA/IPAC Extragalactic Database (NED) which is operated by the Jet Propulsion Laboratory, California Institute of Technology, under contract with the National Aeronautics and Space Administration.

REFERENCES

- Abdo, A. A., Ackermann, M., Ajello, M., et al. 2009a, *ApJ*, 699, 976
 Abdo, A. A., Ackermann, M., Ajello, M., et al. 2009b, *ApJ*, 707, L142
 Ai, Y. L., Yuan, W., Zhou, H. Y., et al. 2010, *ApJ*, 716, L31
 Boller, Th., Brandt, W. N., & Fink, H. 1996, *A&A*, 305, 53
 Cutri, R. M., Wright, E. L., Conrow, T., et al. 2012, *VizieR Online Data Catalog*, 2311
 D'Ammando, F., Orienti, M., Finke, J., et al. 2012, *MNRAS*, 426, 317
 Foschini, L. 2011, *Narrow-Line Seyfert 1 Galaxies and their Place in the Universe*
 Gallo, L. C., Edwards, P. G., Ferrero, E., et al. 2006, *MNRAS*, 370, 245
 Ghisellini, G., Padovani, P., Celotti, A., & Maraschi, L. 1993, *ApJ*, 407, 65
 Giommi, P., & Padovani, P. 1994, *MNRAS*, 268, L51
 Ho, L. C., & Ulvestad, J. S. 2001, *ApJS*, 133, 77
 Hoffman, D. I., Cutri, R. M., Masci, F. J., et al. 2012, *AJ*, 143, 118
 Ivezić, Ž., Smith, J. A., Miknaitis, G., et al. 2007, *AJ*, 134, 973
 Kellermann, K. I., & Pauliny-Toth, I. I. K. 1969, *ApJ*, 155, L71
 Kellermann, K. I., Sramek, R., Schmidt, M., Shaffer, D. B., & Green, R. 1989, *AJ*, 98, 1195
 Komossa, S., Voges, W., Xu, D., et al. 2006, *AJ*, 132, 531
 Laor, A., & Draine, B. T. 1993, *ApJ*, 402, 441
 Leighly, K. M. 1999, *ApJS*, 125, 317
 Liu, H., Wang, J., Mao, Y., & Wei, J. 2010, *ApJ*, 715, L113
 Nieppola, E., Tornikoski, M., & Valtaoja, E. 2006, *A&A*, 445, 441
 Osterbrock, D. E., & Pogge, R. W. 1985, *ApJ*, 297, 166
 Perlman, E. S., Padovani, P., Giommi, P., et al. 1998, *AJ*, 115, 1253
 Peterson, B. M. 2001, *Advanced Lectures on the Starburst-AGN*, 3
 Pogge, R. W. 2000, *New A Rev.*, 44, 381
 Sesar, B., Ivezić, Ž., Lupton, R. H., et al. 2007, *AJ*, 134, 2236
 Shen, Y., Richards, G. T., Strauss, M. A., et al. 2011, *ApJS*, 194, 45
 Shi, G., & Shan, H.-G. 2011, *Progress in Astronomy*, 29, 452
 Sulentic, J. W., Zwitter, T., Marziani, P., & Dultzin-Hacyan, D. 2000, *ApJ*, 536, L5
 Ulrich, M.-H., Maraschi, L., & Urry, C. M. 1997, *ARA&A*, 35, 445
 Wagner, S. J., & Witzel, A. 1995, *ARA&A*, 33, 163
 Wright, E. L., Eisenhardt, P. R. M., Mainzer, A. K., et al. 2010, *AJ*, 140, 1868
 Yuan, W., Zhou, H. Y., Komossa, S., et al. 2008, *ApJ*, 685, 801 (Y08)
 Yuan, W., Liu, B. F., Zhou, H., & Wang, T. G. 2010, *ApJ*, 723, 508
 Zhou, H.-Y., & Wang, T.-G. 2002, *Chinese J. Astron. Astrophys.*, 2, 501
 Zhou, H.-Y., Wang, T.-G., Dong, X.-B., Zhou, Y.-Y., & Li, C. 2003, *ApJ*, 584, 147
 Zhou, H.-Y., Wang, T.-G., Dong, X.-B., Li, C., & Zhang, X.-G. 2005, *Chinese J. Astron. Astrophys.*, 5, 41
 Zhou, H., Wang, T., Yuan, W., et al. 2006, *ApJS*, 166, 128
 Zhou, H., Wang, T., Yuan, W., et al. 2007, *ApJ*, 658, L13